Photochemistry and Photobiology, 2010, 86: 981–989

TiO_2 Nanotubes as a Therapeutic Agent for Cancer Thermotherapy

Chongmu Lee*[1], Chanseok Hong[1], Hohyeong Kim[1], Jungwoo Kang[1] and Hong Mei Zheng[2]

[1]Department of Materials Science and Engineering, Inha University, Incheon, Korea
[2]Department of Biomedical Sciences and Internal Medicine, College of Medicine, Inha University, Incheon, Korea

Received 1 November 2009, accepted 22 February 2010, DOI: 10.1111/j.1751-1097.2010.00731.x

ABSTRACT

We report the photothermal properties as well as the *in vitro* cell test results of titanium oxide nanotubes (TiO_2 NTs) as a potential therapeutic agent for cancer thermotherapy in combination with near-infrared (NIR) light. TiO_2 NTs are found to have a higher photothermal effect upon exposure to NIR laser than Au nanoparticles and single-wall carbon nanotubes, which have also attracted considerable interest as therapeutic agents for cancer thermotherapy. The temperature increase of a TiO_2 NT/NaCl suspension during NIR laser exposure is larger than that of a TiO_2 NT/D.I. water suspension due to the heat generated by the formation of Na_2TiF_6. According to the *in vitro* cell test results the cells exposed to NIR laser without TiO_2 NT treatment have a cell viability of 96.4%. Likewise, the cells treated with TiO_2 NTs but not with NIR irradiation also have a cell viability of 98.2%. Combination of these two techniques, however, shows a cell viability of 1.35%. Also, the cell deaths are mostly due to necrosis but partly due to late apoptosis. These results suggest that TiO_2 NTs can be used effectively as therapeutic agents for cancer thermotherapy due to their excellent photothermal properties and high biocompatibility.

INTRODUCTION

In recent years, thermotherapy techniques based on inorganic nanomaterials and near-infrared (NIR) light have attracted significant interest due to their advantages over conventional surgical treatments. The inorganic nanomaterials currently used as thermal coupling agents in thermotherapy are gold nanoparticles (Au NPs) (1–10), gold nanorods (11–14), gold nanoshells (15–18), gold nanocages (19,20), gold nanocrystals (21,22), single wall carbon nanotubes (SWCNTs) (23–25) and porous silicon (26,27). The advantages of thermotherapy include the anticipated decrease in morbidity and mortality, low cost, suitability for real-time imaging guidance and the ability to perform ablative procedures on outpatients due to its noninvasive nature (15). Thermotherapy is similar to photodynamic therapy (PDT) (28,29) currently used in the clinic in that the combination of a drug (therapeutic agent) and light is used to cause selective damage to the target tissue, but differs from PDT in that the former uses thermal energy whereas the latter uses reactive oxygen species (30) in destroying tumor cells. Recently PDTs for cancer using various inorganic nanomaterials (30–32) including carbon nanoparticles (33–36) have also been reported.

For the irreversible destruction of cancer cells, thermotherapy requires a heat treatment at temperatures $>46°C$ for more than 60 min. However, increasing the treatment temperature can reduce the time needed to induce cytotoxicity (37). In conventional thermotherapy based on simple heating most treatment failures result from insufficient increases in temperature in tumor tissues (38). Therefore, it is very important to develop a thermal coupling agent for thermotherapy with a high photothermal effect in order to secure the irreversible destruction of tumor cells in a short time without damaging the adjacent healthy cells. This paper reports the *in vitro* cell and *in vivo* animal test results as well as the photothermal properties of TiO_2 NTs, and proposes TiO_2 NTs as a potential therapeutic agent used in combination with NIR light in thermotherapy. TiO_2 is a highly functional material with many interesting properties. The use of TiO_2 NTs in drug delivery applications has been reported recently (39,40). However, there are no reports on the application of TiO_2 NTs to cancer thermotherapy. TiO_2 NTs are known to be highly biocompatible (41–45) and easily prepared by the simple electrochemical anodization of titanium (46).

MATERIALS AND METHODS

Materials. The TiO_2 NT samples used in these experiments were in a fragmented state. First, TiO_2 NT layers were formed by the electrochemical anodization of a Ti thin foil in an electrolyte consisting of 0.3 wt% NH_4F and 2 vol.% H_2O in ethylene glycol at 60 V for 17 h. The inner diameter of the TiO_2 NTs was ~100 nm and the thickness of the TiO_2 NT layers was ~160 μm (Fig. 1a,b). The TiO_2 NT layers were fragmented into numerous small pieces with sizes <220 nm (Fig. 2) using an ultrasonicator (Model: 2510E-DTH; BRANSON Ultrasonics Corp.) and filtered through a 220 nm microfilter (Model: SLGV 033 RS; Millipore). Commercial Au NPs and SWCNTs were used as samples for absorbance and photothermal property (ΔT) measurements. The details are as follows:

1. Dry Au NPs (size: 50 nm; Nanocs) were used for the measurements of the absorbance and ΔT to exclude the effect of moisture on the absorbance and ΔT.
2. The SWCNTs used for the absorbance and ΔT measurements are the dry ones (model ASP-100F; Iljin Nanotech Co., Korea) synthesized by using an arc-discharge technique. The purity, diameter and length of the SWCNTs were 90 vol.% (60–70 wt%), 1–1.2 nm and 5–20 μm, respectively.

The weight of each nanomaterial sample used in these experiments was fixed at 12 mg except for the dry Au NP sample (~1 mg).

*Corresponding author email: cmlee@inha.ac.kr (Chongmu Lee)

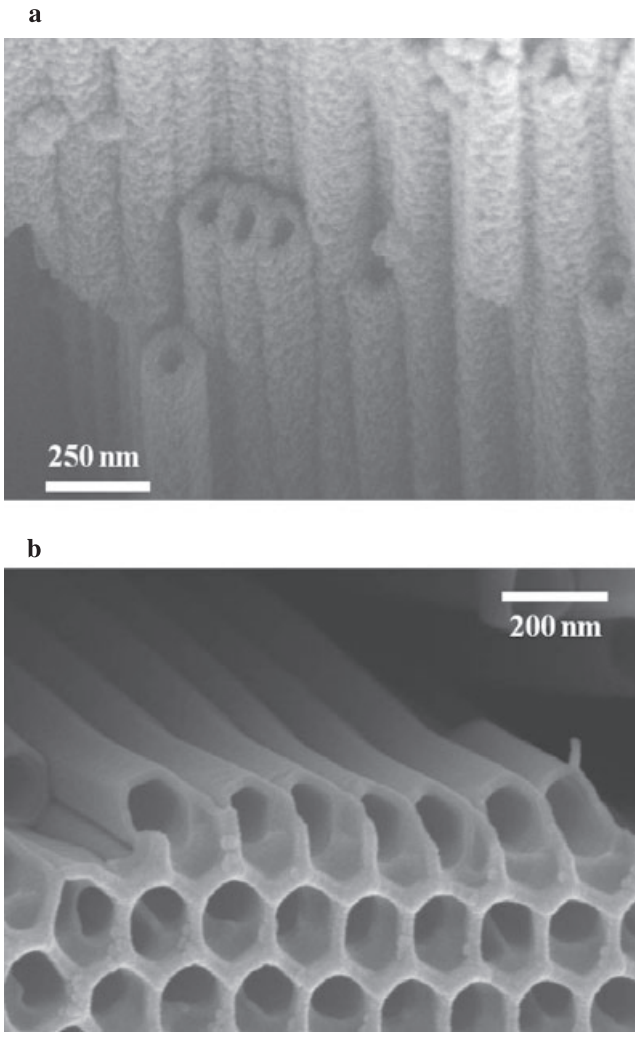

Figure 1. SEM images of TiO_2 NTs: (a) cross-sectional view and (b) bird's eye view. The TiO_2 NTs were formed by anodic etching of Ti thin foils in an electrolyte containing 0.3 wt% NH_4F and 2 vol.% H_2O in ethylene glycol at 60 V for 17 h.

The TiO_2 NT/NaCl suspensions were prepared by mixing TiO_2 NTs with a 9% saline solution, ultrasonicating them for 6 h and finally filtering them through a 220 nm filter (model: MILLEX®; GV, Millipore).

Measurement of heating of nanomaterials by NIR irradiation. NIR light irradiation was carried out on the nanomaterial samples including TiO_2 NTs, Au NPs and SWCNTs using a high-power NIR laser (808 nm) source with a water cooling system to examine their photothermal properties. The laser diode bar was coupled into a fiber with a length, core and numerical aperture of 120 cm, 375 μm and 0.22, respectively. The fiber was connected to a laser diode driver (model: KS3-11321-503, BWT Beijing Ltd.) with a maximum power of 10 W. The samples were irradiated continuously with an NIR laser at 300 mW cm^{-2} for 20 min, and the surface temperature of the samples was measured at 30 s intervals using an IR thermometer (model: AZ 9950). The laser beam size and the distance between the laser diode and samples were in the range of 6–10 and 10–30 cm, respectively, depending on the beam size.

Characterization. The absorbance spectra of the nanomaterial samples were obtained using a UV/Vis/IR spectrophotometer (model: UV-2450; Shimadzu, Japan). X-ray diffraction (XRD) and X-ray photoelectron spectroscopy (XPS) were used to identify the reaction products in the TiO_2 NT/NaCl suspension after laser irradiation.

In vitro cell tests. Murine colon cancer cell lines (CT-26) were cultured in Dulbecco's modified Eagle's medium (DMEM). After

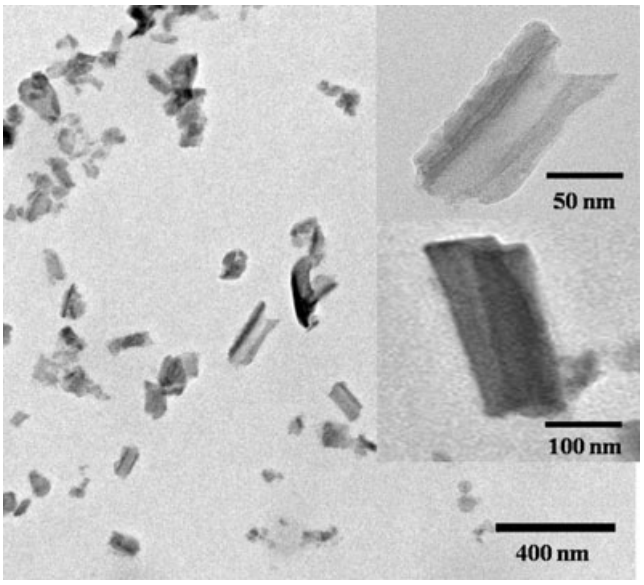

Figure 2. TEM image of the TiO_2 NT fragments with sizes ≤220 nm prepared by ultrasonication and filtration through a 220 nm microfilter.

seeding the cells on 24-well plates, the cells (1×10^5) were incubated for ~24 h at 37°C and in an atmosphere containing 5% CO_2. After incubation, the cell media were removed from the wells, and the cells were washed with PBS. Incomplete DMEM was then added to each well. The TiO_2 NT/NaCl suspension was added to each well. The detached CT-26 cells with or without the incubation treatment in the TiO_2 NT/NaCl suspension were transferred to a circular quartz cuvette and exposed to an NIR laser. A set of cell samples given different treatments were prepared as follows under NIR laser irradiation and another set in the dark (without laser irradiation):

1. control cells (not treated with TiO_2 NTs)
2. the cells treated with 110 mg of the TiO_2 NT/4 mL NaCl suspension
3. the cells treated with 210 mg of the TiO_2 NT/4 mL NaCl suspension (The weights of the TiO_2 NTs were measured prior to filtration. Therefore, their actual weights after filtration may be somewhat lower.) Three different plates were used for each cell sample set: The cells on the bottom of the wells in one plate were stained with 0.4% trypan blue dye (Sigma Aldrich) to determine the level of cell damage before and after exposure to the NIR laser. Another plate was used for the 3-(4,5-dimethyl-2-thiazolyl)-2,5-diphenyl-2H-tetrazolium bromide (MTT) assay, and the other was used to observe the extent of cell death after NIR laser irradiation.

The MTT assays were performed to monitor the cell viability after NIR laser irradiation with an illumination intensity of 300 mW cm^{-2} for 20 min. The MTT assay solution was prepared by dissolving 50 mg MTT powders in 10 mL of a PBS solution and filtering the mixed solution. After removing the cell medium, 180 μL of incomplete medium was added. Subsequently, 20 μL of the MTT solution was added to each cell sample and allowed to incubate for 4 h at 37°C and 5% CO_2 in DMEM. After removing the solution, 200 μL dimethyl sulfoxide was added to each cell sample. After pipetting and shaking, the solution absorbance was examined at a wavelength of 570 nm.

Another kind of *in vitro* cell test, Annexin V-fluorescein isothiocyanate (FITC) Apoptosis assays were performed on five different mouse CT-26 cell sample groups to see their modes of cell deaths: the CT-26 cell control group given neither TiO_2 NTs nor laser treatment, the CT-26 cell group not treated with TiO_2 NTs but with laser, the group not treated with laser but with TiO_2 NTs, the group treated with both a low concentration (110 mg/4 mL)-TiO_2 NT/NaCl suspension and laser, and the group treated with both a high concentration (210 mg/4 mL)-TiO_2 NT/NaCl suspension and laser to distinguish between apoptosis and necrosis. For Annexin V-FITC Apoptosis assay, the TiO_2 NT layer formed by the electrochemical anodization of a Ti thin foil was fragmented into fine particles by ultrasonication for 24 h in a beaker filled with ethanol and then filtered through a 220 nm

filter, first. After evaporation of the ethanol, TiO_2/NaCl-polyethylene glycol (PEG) suspensions with two different concentrations (110 mg/4 mL and 210 mg/4 mL) were prepared by mixing the TiO_2 particles with a 1:1 NaCl-PEG solution. CT-26 cells were then treated with one of the two TiO_2/NaCl:PEG suspensions and then NIR laser at 300 mW cm^{-2} for 20 min, 2×10^6 cells were removed from the culture, washed twice with cold PBS, and double stained with Annexin V-FITC and propidium iodide (PI) (BD Biosciences, San Jose, CA) in Annexin-binding buffer, followed by analysis on a FACScalibur flow cytometer (Becton Dickinson, San Jose, CA) equipped with a 488 nm argon laser. To avoid nonspecific fluorescence from dead cells, live cells were gated using forward and side scatter.

RESULTS

Photothermal effect of TiO_2 NTs

Figure 3 shows a comparison of the photothermal effect of TiO_2 NTs with those of Au NPs and SWCNTs. The TiO_2 NTs showed a larger increase in temperature (ΔT) than the Au NPs and SWCNTs. The inner diameter of the TiO_2 NTs used in this experiment was ~100 nm. On the other hand, the diameter and length of the SWCNTs were 1–1.2 nm and 5–20 μm, respectively, and the average diameter of the Au NPs was 50 nm. Therefore, the surface-to-volume ratio of the TiO_2 NTs is lower than those of the Au NPs and SWCNTs. This high photothermal effect of TiO_2 NTs may be closely related to their high optical absorbance because the absorbance of the TiO_2 NTs is approximately 1.5 and 7 times as high as those of the SWCNTs and Au NPs, respectively (Fig. 4).

Photothermal effect of TiO_2 NT/NaCl suspension

The ΔT in the TiO_2 NT/NaCl suspension strongly depends on the illumination intensity of the NIR laser. The temperature of the TiO_2 NT/NaCl suspension increased to ~60 and ~66°C after 3 and 4 min exposure to the NIR laser at 600 mW cm^{-2}, respectively, while the control increased to ~42°C after 4 min at the same illumination intensity. If a cancer thermotherapy is to be practically used in the clinic, it must be able to destroy cancer cells irreversibly by continuous laser radiation without causing much pain to the patients who have been injected intravenously with the therapeutic agent before the laser treatment. As we can regard the temperature of D.I. water (control) as the temperature of human skin and the temperature of the cancer cells internalized with the TiO_2 NT/NaCl suspension is the same as that of the suspension, most cancer cells can be destroyed irreversibly by continuous radiation of an NIR laser at 600 mW cm^{-2} for more than ~4 min or at 300 mW cm^{-2} for more than ~15 min without causing pain to the patients who have previously been injected intravenously with the TiO_2 NT/NaCl suspension as a therapeutic agent before the laser treatment. Figure 5 suggests the ΔTs of the TiO_2 NT/NaCl suspension and TiO_2 NT/PBS suspension are ~4 and ~3°C larger than that of the TiO_2 NTs/D.I. water suspension, respectively, after 20 min exposure to the NIR laser. In other words, mixing TiO_2 NTs with a NaCl or PBS solution has some additional heating effect. In addition, the ΔT of the TiO_2 NT suspension (the TiO_2 NT fragments in aqueous solution such as D.I. water, NaCl or PBS) was somewhat smaller than that of the TiO_2 NT fragments not mixed with the aqueous solution, which suggests that the aqueous solution surrounding the TiO_2 NT fragments acts as a heat sink absorbing some of the heat generated by the TiO_2 NTs during NIR laser exposure.

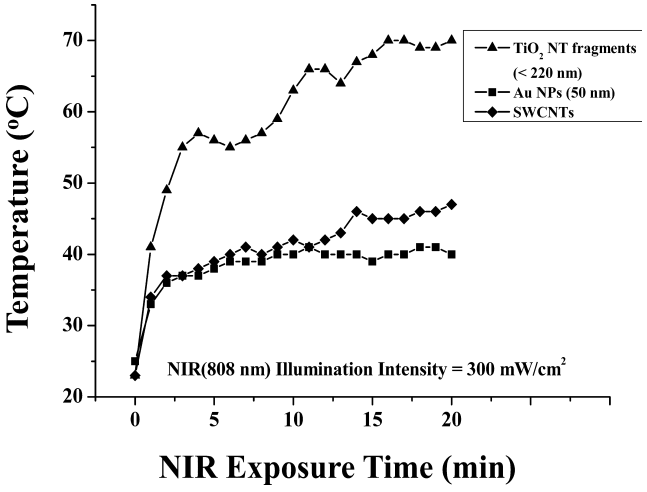

Figure 3. Comparison of the temperature of TiO_2 NTs with those of other inorganic nanomaterials such as Au NPs and SWCNTs which have recently been reported to be potential therapeutic agents for cancer thermotherapy during NIR laser irradiation at illumination intensities of 300 mW cm^{-2}. TiO_2 NT, Au NP and SWCNT samples are not in a state of suspension but are all in a state of dry solid; in other words, they have equal concentrations (100%). The TiO_2 NT samples have been prepared by immersing the TiO_2 NT layer formed on a Ti thin foil in D. I. water followed by ultrasonicating for 5 h in an ultrasonicator and baking it in an oven at 200°C for 2 h. Au NP and SWCNT samples are the dry ones purchased from Nanocs and Iljin Nanotech Co.

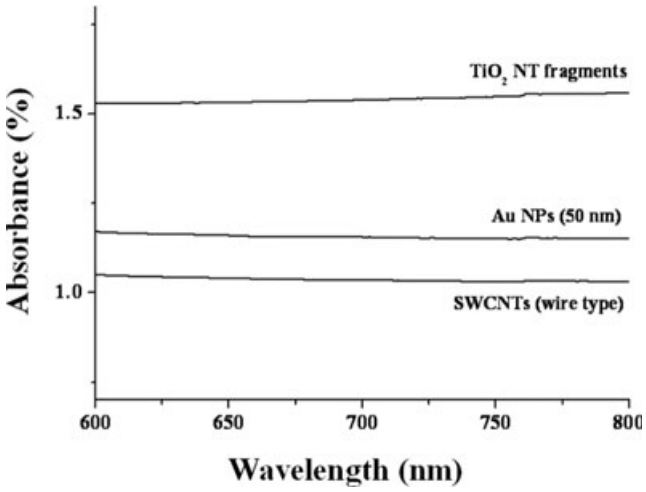

Figure 4. Absorbance spectra of some inorganic nanomaterials as potential therapeutic agents for cancer thermotherapy. The TiO_2 NT, Au NP and SWCNT samples used in the absorbance measurements (Fig. 3) are exactly the same as those in Fig. 2, *i.e.* they have equal concentrations (100%).

XPS and XRD analyses of TiO_2 NT/NaCl suspension

We found through a simple experiment that there was almost no difference in ΔT during exposure to NIR laser between NaCl solution and pure D.I. water. This experimental result suggests that NaCl itself does not give rise to any particular photothermal effect. Hence, XPS and XRD analyses were performed to determine the origin of the additional heating

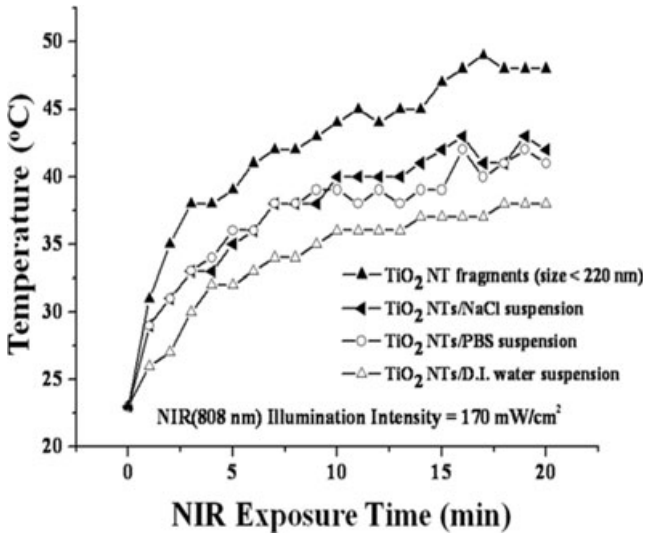

Figure 5. Temperatures of TiO_2-based nanomaterials during exposure to NIR laser at 170 mW cm^{-2}. All the concentrations of the TiO_2-based nanomaterials except the TiO_2 NT fragments used in these measurements are equal (210 mg/4 mL).

effect of the TiO_2 NT/NaCl suspension upon exposure to the NIR laser.

The XPS spectra of TiO_2 NT/NaCl suspension after exposure to NIR laser at 170 mW cm^{-2} for 20 min are shown in Fig. 6. The binding energies of the main peaks in the XPS spectra are given in Table 1 along with those of the candidate compounds. The additional heating effect of the TiO_2 NT/NaCl suspension is probably attributed to the formation of Na_2TiF_6, Na_2CO_3, Na_2O or $TiCl_4$ among the candidate compounds in Table 1 as their binding energy values coincide well with those of two or more main intensity peaks in the XPS spectra. The presumable chemical reactions for formation of those compounds and the enthalpy changes of the reactions (ΔH°) are as follows:

$$2NaCL(s) + TiO_2(s) + 6NH_4F(l) = Na_2TiF_6(s) + 2HCl(l) + 2H_2O(l) + 6NH_3(l) : \Delta H^\circ = ? \quad (1)$$

$$NaCl(s) + C(s) + 3HCl(l) = Na_2CO_3(s) + 2HCl(l) + 2H_2(g) : \Delta H^\circ = 51.08 \text{ kcal mol}^{-1} \quad (2)$$

$$2NaCl(s) + H_2O(l) = Na_2O(s) + 2HCl(l) : \Delta H^\circ = 85.34 \text{ kcal mol}^{-1} \quad (3)$$

$$2NaCl(s) + TiO_2(s) = 2Na_2O(s) + TiCl_4(l) : \Delta H^\circ = 232.82 \text{ kcal mol}^{-1} \quad (4)$$

The ΔH° values were calculated by using the enthalpy change data (47) in Tables 2–5. NH_4F in reaction (2) may originate from the NH_4F anodization solution used to synthesize the TiO_2 NTs and carbon in reaction (3) is contaminant atoms commonly found in the XPS spectra of most materials. The positive value of ΔH° of reactions (3)–(5) indicate the formation reactions of Na_2CO_3, Na_2O and $TiCl_4$ are endothermic.

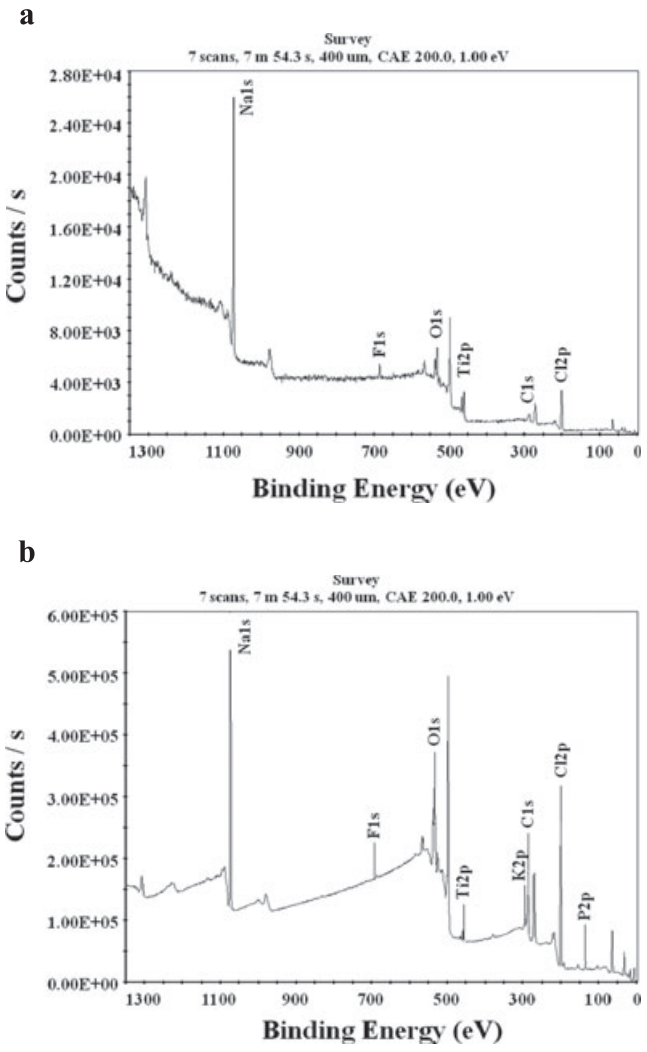

Figure 6. XPS spectra of (a) the TiO_2 NT/NaCl suspension and (b) the TiO_2 NT/PBS suspension after exposure to NIR laser at 170 mW cm^{-2} for 20 min. The concentrations of TiO_2 NTs in TiO_2 NT/NaCl suspensions were measured before filtration.

Table 1. Details of the main peaks in the XPS spectra of the TiO_2 NT/NaCl suspension after NIR laser irradiation at 170 mW cm^{-2} for 20 min along with relevant compounds.

TiO_2 NT/NaCl suspension		Candidates	
Elemental identification name	Peak binding energy (eV)	Compound name	Binding energy (eV)
Na_{1S}	1073.21	Na_2CO_3	1071.7
		Na_2TiF_6	1071.6
		Na_2O	1072.5
Ti_{2p}	460.05	$TiCl_4$	458.5
C_{1s}	287.00	Na_2CO_3	289.4
F_{1s}	685.75	Na_2TiF_6	685.3
O_{1s}	531.81	Na_2O	529.7
		Na_2CO_3	531.6
Cl_{2p}	200.45	$TiCl_4$	198.2

NT = nanotube.

Table 2. Heat of formation of the substances involved in the chemical reaction of Na_2TiF_6 formation (47).

Substance	NaCl (s)	TiO_2 (s)	NH_4F (l)	Na_2TiF_6 (s)	HCl (l)	H_2O (l)	NH_3 (l)
Heat of formation ΔH_f^o (kcal mol^{-1})	−98.23	−218.0	−110.40	?	−40.02	−68.32	−19.32

Table 3. Heat of formation of the substances involved in the chemical reaction of Na_2CO_3 formation (47).

Substance	NaCl (s)	C (s)	H_2O (l)	Na_2CO_3 (s)	HCl (l)	H_2 (g)
Heat of formation ΔH_f^o (kcal mol^{-1})	−98.23	0	−68.32	−270.3	−40.02	0

Table 4. Heat of formation of the substances involved in the chemical reaction of Na_2O formation (47).

Substance	NaCl (s)	H_2O (l)	Na_2O (s)	HCl (l)
Heat of formation ΔH_f^o (kcal mol^{-1})	−98.23	−68.32	−99.4	−40.02

Table 5. Details of the main peaks in the XPS spectra of the TiO_2 NT/PBS suspension after NIR irradiation at 170 mW cm^{-2} for 20 min along with relevant compounds.

TiO_2 NT/PBS suspension		Candidates	
Elemental identification name	Peak binding energy (eV)	Compound name	Binding energy (eV)
Na_{1S}	1071.97	Na_2CO_3	1071.7
		Na_2TiF_6	1071.6
		Na_2O	1072.5
Ti_{2p}	457.08	$TiCl_4$	458.5
C_{1s}	285.10	Na_2CO_3	289.4
F_{1s}	692.08	Na_2TiF_6	685.3
O_{1s}	531.72	Na_2O	529.7
		Na_2CO_3	531.6
Cl_{2p}	199.26	$TiCl_4$	198.2
P_{2p}	133.08	Na_2HPO_4	133.1
		NaH_2PO_4	134.2

XPS = X-ray photoelectron spectroscopy; NT = nanotube; NIR = near-infrared.

On the other hand, we could not calculate the ΔH^o of reaction (2) as we failed to find the heat of formation data of Na_2TiF_6, unfortunately. Nevertheless, we strongly believe that the Na_2TiF_6 formation reaction is exothermic as the formation enthalpy changes for most compounds containing both Na and Ti are known to be negative like Na_2SiF_6:

$$2Na^+ + 2Cl^- + SiF_4(g) + 2HF(aq) = Na_2SiF_6(c) + 2HCl(aq) : \Delta H^\circ = -32.33 \text{ kcal mol}^{-1} \quad (5)$$

where SiF_4 and HF may originate from the HF/C_2H_5OH anodization solution used for fabrication of porous silicon. SiF_4 represents a chemical reaction product of Si and HF. The additional heating effect in reaction (2) seems to be obtained because the amount of heat generated by reaction (1) is larger than the total amount of heat absorbed by reactions (3)–(5). Therefore, we may conclude that the additional heating effect in the TiO_2 NT/NaCl suspension upon exposure to NIR laser originates from formation of Na_2TiF_6.

XRD analysis results confirm the formation of Na_2TiF_6 during NIR laser irradiation. Comparison of the XRD pattern before laser irradiation (Fig. 7a) with that after laser irradiation (Fig. 7b) clearly show that Na_2TiF_6 was newly formed

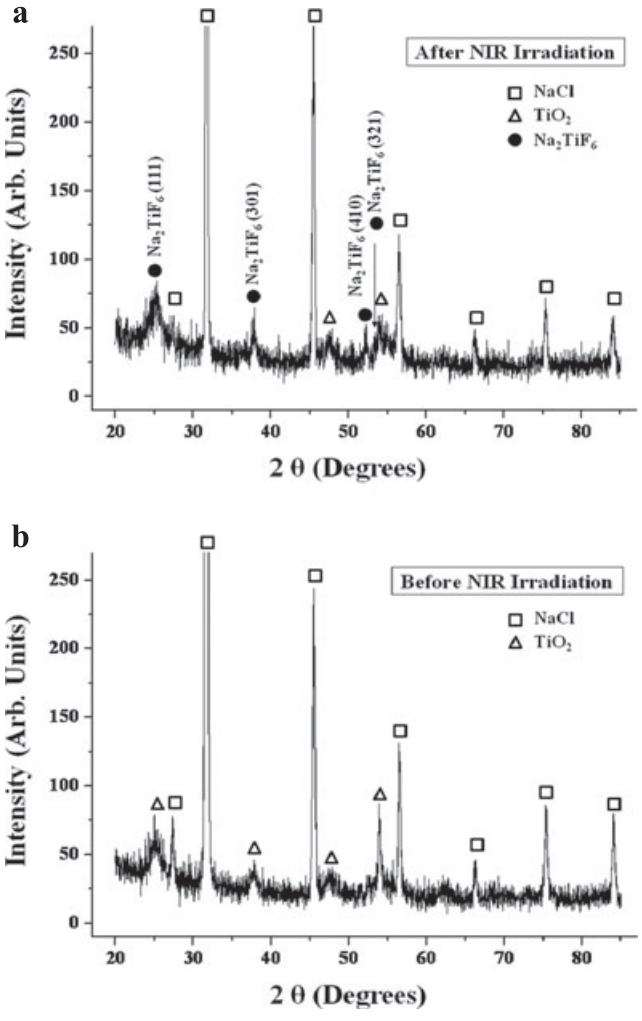

Figure 7. X-ray diffraction patterns of theTiO_2 NT/NaCl suspension (a) after and (b) before NIR laser irradiation at 300 mW cm^{-2} for 20 min.

by NIR laser irradiation. No crystalline material except TiO_2 and NaCl is observed in the TiO_2 NT/NaCl suspension before NIR laser irradiation. However, Na_2TiF_6 as well as TiO_2 and NaCl are observed after irradiation.

The XPS spectrum of the TiO_2 NT/PBS suspension shown in Fig. 6b is very similar to that of the TiO_2 NT/NaCl suspension in Fig. 5a, as can be expected from the composition of the PBS solution (10.9 g Na_2HPO_4, 3.2 g NaH_2PO_4, 90 g NaCl, 1000 mL D.I. water) used in this experiment. The only difference between the XPS spectrum of the TiO_2 NT/NaCl suspension (Fig. 5a) and that of the TiO_2 NT/PBS suspension (Fig. 5b) is that the former has an additional peak of P_{2p} as indicated by a comparison of the details of the main peaks in the XPS spectra with Tables 1 and 5. The P_{2p} peak has turned out to originate from Na_2HPO_4 and NaH_2PO_4 in the PBS solution as a result of identification of compounds based on the binding energy value of the P_{2p} peak. Therefore, we may conclude that the additional heating effect in the TiO_2 NT/PBS suspension upon exposure to NIR laser also originates from the formation of Na_2TiF_6 as in the TiO_2 NT/NaCl suspension. The slightly smaller ΔT of the TiO_2 NT/PBS suspension than that of the TiO_2 NT/NaCl suspension shown in Fig. 4 may be due to the lower NaCl concentration in the PBS solution than in the NaCl solution, which leads to the formation of a smaller amount of Na_2TiF_6 upon exposure to the NIR laser.

In vitro cell tests

MTT assays were performed on mouse CT-26 cells to examine localized photothermal destruction of cancer cells. Figure 8 shows that the CT-26 cells treated with both the TiO_2 NT/NaCl suspension and NIR laser were killed effectively. The assay suggests that the cells treated with TiO_2 NT/NaCl suspension with a higher TiO_2 NT concentration and laser

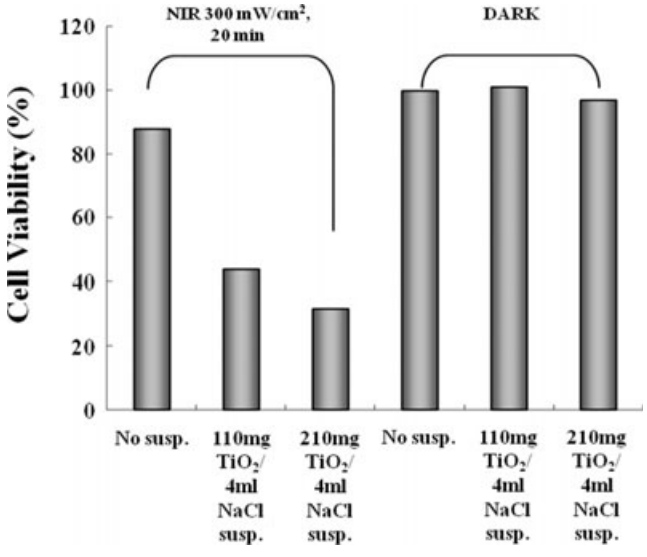

Figure 8. MTT assay results. NIR laser irradiation was performed with an illumination intensity of 300 mW cm^{-2} for 20 min. The CT-26 cells treated with both TiO_2 NT/NaCl suspension and NIR laser were effectively killed. In contrast, those treated with only the TiO_2 NT/NaCl suspension or those treated with only NIR laser were not nearly killed.

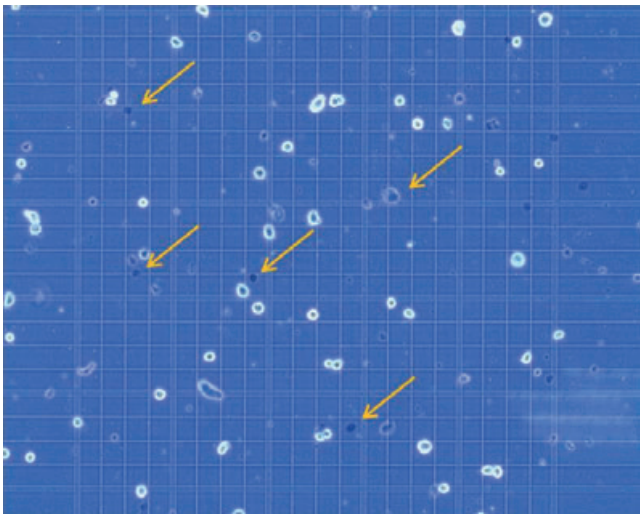

Figure 9. Optical microscopy images showing the *in vitro* cell test results on CT-26 murine colon cancer cells treated with the TiO_2 NT/NaCl suspension and NIR laser at 300 mW cm^{-2} for 20 min after NIR laser exposure. The cells were stained with trypan blue dye after the NIR laser treatment to examine the level of cell damage. The cells indicated by the arrows are some examples of those that turned blue after staining.

treatment have a markedly higher death rate than that with a lower concentration. On the other hand, all three samples with different concentrations had a cell death rate of zero in the dark. Figure 9 shows high-magnification optical microscopy images of the cells dispersed in the TiO_2 NT/NaCl suspension given the laser treatment. The cells were stained with trypan blue dye after exposure to the NIR laser to examine the extent of cell damage. The fact that the cells turned blue suggests that they were dead. Obviously higher cell death rates would have been achieved if the NIR laser with a higher illumination intensity had been used in this test. The MTT assay results confirm that only the technique combined with the TiO_2 NT/NaCl suspension and NIR laser exposure leads to cell death.

The fluorescent-activated cell sorter flow cytometry profiles (Fig. 10a) obtained as a result of Annexin V-FITC Apoptosis assay represent Annexin V-FITC staining in the *X*-axis and PI in the *Y*-axis. The four sections of the quadrant in each profile from the upper left in a clockwise direction represent necrosis, late apoptosis, early apoptosis and live cell, respectively. The groups treated with TiO_2 NT/NaCl suspensions show substantially higher cell death (necrosis + late apoptosis) rates than those not given both treatments (Fig. 10a). The Annexin V-FITC Apoptosis assay results in Fig. 10a are summarized in Fig. 10b. The group exposed to NIR laser at 300 mW cm^{-2} for 20 min without TiO_2 NT treatment shows a cell viability of 96.4%. Likewise, the group treated with TiO_2 NTs but not with NIR irradiation also shows a cell viability of 98.2% (Fig. 10b). Combination of these two techniques, however, shows cell viabilities of 4.81% and 1.35% for lower and higher TiO_2 NT concentrations, respectively, implying that most cells are killed. The cell deaths are mostly due to necrosis but partly due to late apoptosis. These results suggest that only a combination of both TiO_2 NTs and NIR laser treatments can kill cells and that a higher TiO_2 NT concentration results in a

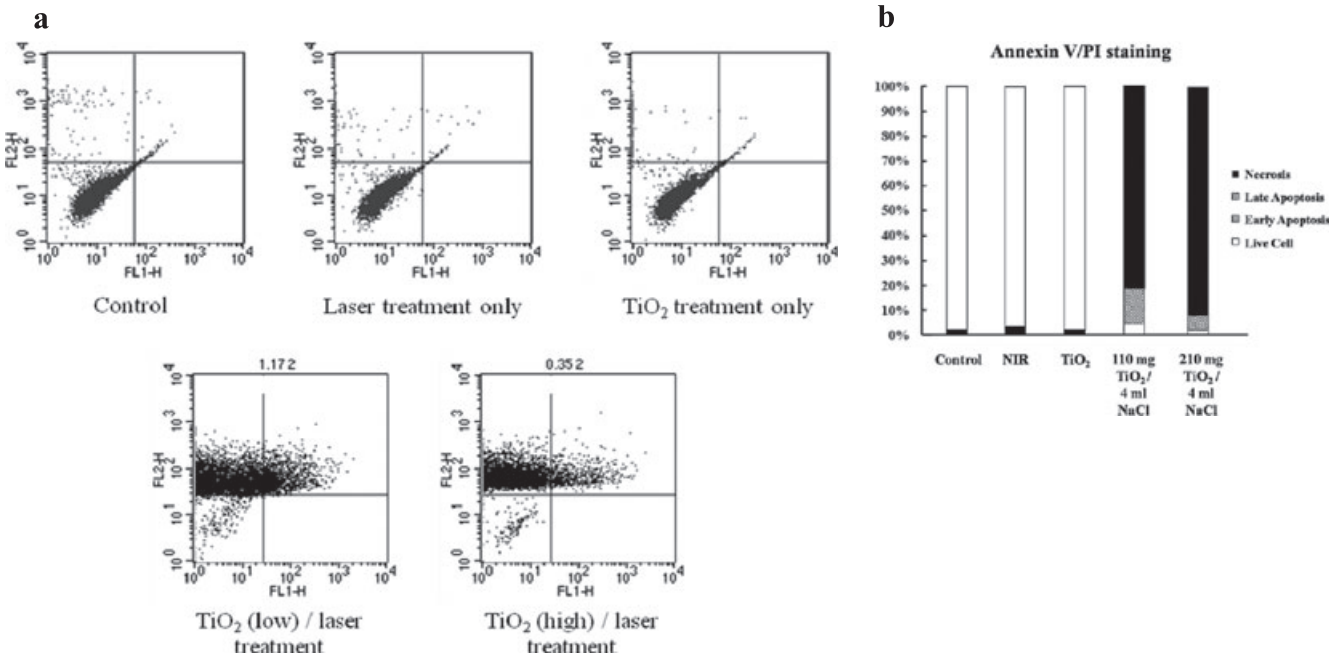

Figure 10. (a) Fluorescent-activated cell sorter flow cytometry profiles obtained as a result of Annexin V-FITC Apoptosis assay for five different mouse CT-26 cell sample groups to see their modes of cell deaths: the CT-26 cell control group given neither TiO_2 NTs nor laser treatment, the CT-26 cell group not treated with TiO_2 NTs but with laser, the group not treated with laser but with TiO_2 NTs, the group treated with both a lower concentration (110 mg/4 mL)-TiO_2 NT/NaCl suspension and laser, and the group treated with both a higher concentration (210 mg/4 mL)-TiO_2 NT/NaCl suspension and laser to distinguish between apoptosis and necrosis. The NIR laser irradiation intensity and time in the treatments were 300 mW cm^{-2} and 20 min, respectively. (b) Summary of the Annexin V-FITC Apoptosis assay results showing the percentages of cell death modes: necrosis, late apoptosis, early apoptosis and live cell.

higher cell death rate, particularly a higher necrosis rate than a lower TiO_2 NT concentration.

DISCUSSION

The temperature increase (ΔT) of a nanomaterial sample during NIR laser irradiation may be expressed as

$$\Delta T = [\eta A(1 - R(\lambda))I_o(1 - \exp(-\alpha d))]/mCp \qquad (6)$$

where η is the efficiency of the conversion of the energy absorbed into heat in the sample, $R(\lambda)$ is the surface reflectivity of the sample depending on the wavelength of the incident NIR laser. A and d are the surface area and thickness of the sample, respectively, α and C_p are the absorption coefficient and specific heat of the sample, respectively, and I_o is the intensity of the incident NIR laser. αd corresponds to the absorbance of the sample because the absorbance is proportional to the absorption coefficient and thickness of a material. m is not simply the whole sample mass because there is a complex relationship between m and the sample mass. Indeed, m depends on not only the sample size but also on the laser spot size and IR thermometer spot size. It is difficult to compare materials directly in terms of the photothermal effect because ΔT depends on the surface area, thickness and mass of the material samples. For a meaningful comparison of the photothermal effects of the materials, the parameters depending on the size and morphology of the materials should be the same for all samples. However, this is almost impossible to achieve in reality. In this work, we examined the relative photothermal effects of TiO_2 NTs with some already reported photothermal nanomaterials by comparing their ΔTs only under the condition of equal concentrations even if the surface area of their samples was not the same.

Our results show that TiO_2 NTs have a higher photothermal effect (a larger ΔT) upon exposure to NIR laser than Au nanoparticles and single-wall carbon nanotubes. ΔT may be influenced most strongly by the absorbance between all the parameters because it changes exponentially only with absorbance while lineally with the other parameters. Therefore, a higher ΔT of the TiO_2 NTs than those of the other two nanomaterials despite its lower surface-to-volume ratio is due mainly to its higher absorbance (Fig. 4). The Au NP samples used to measure the absorbance were wet ones in an aqueous solution, while those used to measure ΔT were dry ones. Therefore, the real absorbance of the Au NPs may be somewhat higher than that of the Au NPs in an aqueous solution. However, we must be conservative for the higher photothermal effect of TiO_2 NTs as the maximum absorptions of the Au NP and SWCNT samples used in this study was not tuned to 808 nm. According to Khlebtsov *et al.* (8), colloidal Au has maximal absorption at 520–550 nm and its absorption is minimal at 808 nm, but for Au nanoshells and nanorods the absorption maximum can be tuned to 808 nm. Thus, the photothermal property of TiO_2 NTs may not be better than the already reported photothermal nanomaterials such as Au nanoshells and nanorods.

In this preliminary study, only the *in vitro* cell tests were conducted with TiO_2 NTs. The *in vitro* cell test results show that the thermotherapy based on TiO_2 NTs combined with

NIR laser is an efficient technique in destroying cancer cells. They do not, however, necessarily show that the TiO_2 NTs can inhibit tumor growth. Therefore, *in vivo* animal tests are underway to check if the TiO_2 NTs can inhibit tumor growth. Another point worth mentioning here is that only the chemical interaction of TiO_2 NTs with NaCl has been investigated in this study, but the interaction of TiO_2 NTs with other blood components, for example albumin, should also be investigated before the TiO_2 NT/NaCl suspension is actually used for cancer treatment in the clinic. There is also a report of some additional damaging effects of TiO_2 nanostructures at visible light radiation (48). According to the report, photocatalytic preoxidation can take place at the TiO_2 surface by heterogeneous-mediated processes leading to cell wall membrane degradation. Thus, the possible side effects should also be thoroughly checked eventually as IR-induced photocatalytic effects might occur.

Acknowledgements—This study was supported by the Korea Engineering and Science Foundation (KOSEF) through the "2007 National Research Lab Program." The authors thank Mina Kim and Heeseung Lee at the College of Medicine, Inha University, for performing the MTT assay and animal tests. Appreciation is also extended to Prof. Soon-Sun Hong and Don-Haeng Lee at the College of Medicine and Wan In Lee at the Department of Chemistry, Inha University, for their valuable discussions and suggestions.

REFERENCES

1. Pitsillides, C. M., E. K. Joe, X. Wei, R. R. Anderson and C. P. Lin (2003) Selective cell targeting with light-absorbing microparticles and nanoparticles. *Biophys. J.* **84**, 4023–4032.
2. Zharov, V. P., V. Galitovsky and M. Viegas (2003) Photothermal detection of local thermal effects during selective nanophotothermolysis. *Appl. Phys. Lett.* **83**, 4897–4899.
3. Zharov, V. P., E. N. Galitovskaya and M. Viegas (2004) Photothermal guidance for selective photothermolysis with nanoparticles. *Proc SPIE* **5319**, 291–300.
4. Hainfeld, J. F., D. N. Slatkin and H. M. Smilowitz (2004) The use of gold nanoparticles to enhance radiotherapy in mice. *Phys. Med. Biol.* **49**, N309–N315.
5. Zharov, V. P., E. N. Galitovskaya, C. Johnson and T. Kelly (2005) Synergistic enhancement of selective nanophoto thermolysis with gold nanoclusters: Potential for cancer therapy. *Lasers Surg. Med.* **37**, 219–226.
6. El-Sayed, I. H., X. Huang and M. A. El-Sayed (2006) Selective laser photo-thermal therapy of epithelial carcinoma using anti-EGFR antibody conjugated gold nanoparticles. *Cancer Lett.* **239**, 129–135.
7. Huang, X., P. K. Jain, I. H. El-Sayed and M. A. El-Sayed (2006) Determination of the minimum temperature required for selective photothermal destruction of cancer cells using immunotargeted gold nanoparticles. *Photochem. Photobiol.* **82**, 412–417.
8. Khlebtsov, B., V. Zharov, A. Melnikov, V. Tuchin and N. Khlebtsov (2006) Optical amplification of photothermal therapy with gold nanoparticles and nanoclusters. *Nanotechnology* **17**, 5167–5179.
9. Terentyuk, G. S., G. N. Maslyakova, L. V. Suleymanova, N. G. Khlebtsov, B. N. Khlebtsov, G. G. Akchurin, I. L. Maksimova and V. V. Tuchin (2009) Laser-induced tissue hyperthermia mediated by gold nanoparticles: Toward cancer phototherapy. *J. Biomed. Opt.* **14**, 021016-1-8.
10. Terentyuk, G. S., G. N. Maslyakova, L. V. Suleymanova, B. N. Khlebtsov, B. Y. Kogan, G. G. Akchurin, A. V. Shantrocha, I. L. Maksimova, N. G. Khlebtsov and V. V. Tuchin (2009) Circulation and distribution of gold nanoparticles and induced alterations of tissue morphology at intravenous particle delivery. *J. Biophoton.* **2**, 292–302.
11. Huang, X., I. H. El-Sayed and M. A. El-Sayed (2006) Cancer cell imaging and photothermal therapy in the near-infrared region by using gold nanorods. *J. Am. Chem. Soc.* **128**, 2115–2120.
12. Takahashi, H., T. Niidome, A. Nariai, T. Niidome and S. Yamada (2006) Gold nanorod-sensitized cell death: Microscopic observation of single living cells irradiated by pulsed near-infrared laser light in the presence of gold nanorods. *Chem. Lett.* **35**, 500–501.
13. Takahashi, H., T. Niidome, A. Nariai, Y. Niidome and S. Yamada (2006) Photothermal reshaping of gold nanorods prevents further cell death. *Nanotechnology* **17**, 4431–4435.
14. Huff, T. B., L. Tong, Y. Zhao, M. N. Hansen, J. K. Cheng and A. Wei (2007) Hyperthermic effects of gold nanorods on tumor cells. *Nanomedicine* **2**, 125–132.
15. Hirsch, L. R., R. L. Stafford, J. A. Baukson, S. R. Sershen, B. Rivera, R. E. Price, J. D. Hazle, N. J. Halas and J. L. West (2003) Nanoshell-mediated near-infrared thermal therapy of tumors under magnetic resonance guidance. *Proc. Natl Acad. Sci. USA* **100**, 13549–13554.
16. Loo, C., A. Lin, L. Hirsch, M. H. Lee, J. Barton, N. Halas, J. West and R. Drezek (2004) Nanoshell-enabled photonics-based imaging and therapy of cancer. *Technol. Cancer Res. Treat.* **3**, 33–40.
17. O'Neal, D. P., L. R. Hirsch, N. J. Halas, J. D. Payne and J. L. West (2004) Photothermal tumor ablation in mice using near infrared absorbing nanoshells. *Cancer Lett.* **209**, 171–176.
18. Loo, C., A. Lowery, N. J. Halas, J. L. West and R. Drezek (2005) Immunotargeted nanoshells for integrated cancer imaging and therapy. *Nano Lett.* **5**, 709–711.
19. Chen, J., B. Wiley, Z. Y. Li, D. Campbell, F. Saeki, H. Cang, L. Au, J.. Lee, X. Li and Y. Xia (2005) Gold nanocages: Engineering their structure for biomedical applications. *Adv. Mater.* **17**, 2255–2261.
20. Hu, M., H. Petrova, J. Chen, J. M. McLellan, A. R. Siekkinen, M. Marquez, X. Li, Y. Xia and G. V. Hartland (2006) Ultrafast laser studies of the photothermal properties of gold nanocages. *J. Phys. Chem. B* **110**, 1520–1524.
21. Link, S. and M. A. El-Sayed (2000) Shape and size dependence of radiative, non-radiative and photothermal properties of gold nanocrystals. *Int. Rev. Phys. Chem.* **19**, 409–453.
22. Link, S. and M. A. El-Sayed (2003) Optical properties and ultrafast dynamics of metallic nanocrystals. *Ann. Rev. Phys. Chem.* **54**, 331–366.
23. Kam, N. W. S., M. O'Connell, J. A. Wisdom and H. Dai (2005) Carbon nanotubes as multifunctional biological transporters and near-infrared agents for selective cancer cell destruction. *Proc. Natl Acad. Sci. USA* **102**, 11600–11605.
24. Zavaleta, C., A. de la Zerda, Z. Liu, S. Keren, Z. Cheng, M. Schipper, X. Chen, H. Dai and S. S. Gambhir (2008) Noninvasive Raman spectroscopy in living mice for evaluation of tumor targeting with carbon nanotubes. *Nano Lett.* **8**, 2800–2805.
25. Panchapakesan, B., S. Lu, K. Sivakumar, K. Taker, G. Cesarone and E. Wickstrom (2005) Single-wall carbon nanotube nanobomb agents for killing breast cancer cells. *Nanobiotechnology* **1**, 133–139.
26. Lee, C., H. Kim, Y. Cho and W. I. Lee (2007) The properties of porous silicon as a therapeutic agent via the new photodynamic therapy. *J. Mater. Chem.* **17**, 2648–2653.
27. Lee, C., H. Kim, C. Hong, M. Kim, S. S. Hong, D. H. Lee and W. I. Lee (2008) Porous silicon as an agent for cancer thermotherapy based on near-infrared light irradiation. *J. Mater. Chem.* **18**, 4790–4795.
28. Dolmans, D. E., D. Fukumura and R. K. Jain (2003) Photodynamic therapy for cancer. *Nat. Rev. Cancer* **3**, 380–387.
29. Triesscheijn, M., P. Baas, J. H. Schellens and F. A. Stewart (2006) Photodynamic therapy in oncology. *Oncologist* **11**, 1034–1044.
30. Hosford, M. E., J. G. Muller and C. J. Burrows (2004) Spermine participates in oxidative damage of guanosine and 8-oxoguanosine leading to deoxyribosylurea formation. *J. Am. Chem. Soc.* **126**, 9540–9541.
31. Wang, S., R. Gao, F. Zhou and M. Selke (2004) Nanomaterials and singlet oxygen photosensitizers: Potential applications in photodynamic therapy. *J. Mater. Chem.* **14**, 487–493 and references therein.

32. Juzenas, P., W. Chen, Y.-P. Sun, M. A. Coelho, R. Generalov, N. Generalova and I. L. Christensen (2008) Quantum dots and nanoparticles for photodynamic and radiation therapies of cancer. *Adv. Drug Deliv. Rev.* **60**, 1600–1614 and references therein.
33. Kratschmer, W., K. Fostiropoulos and D. R. Huffman (1990) The infrared and ultraviolet absorption spectra of laboratory-produced carbon dust: Evidence for the presence of the C(*60*) molecule. *Chem. Phys. Lett.* **170**, 167–170.
34. Foote, C. S. (1994) Photophysical and photochemical properties of fullerenes. *Topics Curr. Chem.* **169**, 347–363.
35. Fraelich, M. R. and R. B. Weisman (1993) Triplet states of fullerene C60 and C70 in solution: Long intrinsic lifetimes and energy pooling. *J. Phys. Chem.* **97**, 11145–11147.
36. Aborgast, J. W., A. P. Darmanyan, C. S. Foote, F. N. Diederich, Y. Rubin, F. Diederich, M. Alvarez, S. J. Anz and R. L. Whetten (1991) Photophysical properties of sixty atom carbon molecule (C60). *J. Phys. Chem.* **95**, 11–12.
37. Goldberg, S. N., G. S. Gazelle and P. R. Mueller (2000) Thermal ablation therapy for focal malignancy. *Am. J. Roentgenol.* **174**, 323–331.
38. Jordan, A., K. Maier-Hauff, P. Wust and M. Johaunsen (2006) Nanoparticles for thermotherapy. In *Nanomaterials for Cancer Therapy* (Edited by C. Kumar), pp. 242–258. Wiley-VCH, Weinheim and references therein.
39. Yao, C., G. Balasundaram and T. Webster (2007) Use of anodized titanium in drug delivery applications. *Mater. Res. Soc. Symp. Proc.* **951E**, 28–29.
40. von Wilmowsky, C., S. Bauer, R. Lutz, M. Meisel, F. W. Neukam, T. Toyoshima, P. Schmuki, E. Nkenke and K. A. Schlegel (2009) In vivo evaluation of anodic TiO_2 nanotubes: An experimental study in the pig. *J. Biomed. Mater. Res.* **89B**, 165–171.
41. Sul, Y. T., C. B. Johansson, Y. Jeong and T. Albrektsson (2001) The electrochemical oxide growth behaviour on titanium in acid and alkaline electrolytes. *Med. Eng. Phys.* **23**, 329–346.
42. Zhang, Y. M., P. Bataillon-Linez, P. Huang, Y. M. Zhao, Y. Han, M. Traisnel, K. W. Xu and H. F. Hildebrand (2004) Surface analyses of micro-arc oxidized and hydrothermally treated titanium and effect on osteoblast behavior. *J. Biomed. Mater. Res.* **68A**, 383–391.
43. Sasaki, K., K. Asanuma, K. Johkura, T. Kasuga, Y. Okouchi, N. Ogiwara, S. Kubota, R. Teng, L. Cui and X. Zhao (2006) Ultrastructural analysis of TiO_2 nanotubes with photodecomposition of water into O_2 and H_2 implanted in the nude mouse. *Ann. Anat.* **188**, 137–142.
44. Jang, J. M., S. J. Park, G. S. Choi, T. Y. Kwon and K. H. Kim (2008) Chemical state and ultra-fine structure analysis of biocompatible TiO_2 nanotube-type oxide film formed on titanium substrate. *Met. Mater. Int.* **14**, 457–464.
45. Garcia-Ripoll, A., A. M. Amat, A. Argues, R. Vicente, M. M. Ballesteros Martin, J. A. Sanchez Perez, I. Oller and S. Malato (2009) Confirming *Pseudomonas putida* as a reliable bioassay for demonstrating biocompatibility enhancement by solar photo-oxidative processes of a biorecalcitrant effluent. *J. Hazard. Mater.* **162**, 1223–1227.
46. Zwilling, V., M. Aucouturier and E. Darque-Ceretti (1999) Anodic oxidation of titanium and TA6V alloy in chromic media. An electrochemical approach. *Electrochim. Acta* **45**, 921–929.
47. Barin, I. (1995) *Thermochemical Data of Pure Substances*, 3rd edn. VCH, Weinheim, New York, Basel, Cambridge, Tokyo.
48. Kiwi, J. and V. Nadtochenko (2004) New evidence for TiO_2 photocatalysis during bilayer lipid peroxidation. *J. Phys. Chem. B* **108**, 17675–17684.